J Mater Sci: Mater Electron (2022) 33:18400–18409

Design of the polyacrylonitrile-reduced graphene oxide nanocomposite-based non-enzymatic electrochemical biosensor for glucose detection

Selcan Karakuş[1,*], Cihat Taşaltın[2], İlke Gürol[2], Gülsen Baytemir[3], and Nevin Taşaltın[3,4,*]

[1] Department of Chemistry, Istanbul University-Cerrahpasa, Istanbul, Turkey
[2] TUBITAK Marmara Research Center, Materials Institute, Gebze, Kocaeli, Turkey
[3] CONSENS Inc., Maltepe University Research Center, Technopark, Maltepe University, Istanbul, Turkey
[4] Department of Basic Sciences, Maltepe University, Istanbul, Turkey

Received: 22 January 2022
Accepted: 29 June 2022
Published online: 15 July 2022

ABSTRACT

With the advantages of developed electronic devices, various biosensor applications have become attractive issues with excellent electrochemical performances against biomarkers and molecules in biomedical applications. In this study, novel polyacrylonitrile (PAN)-reduced graphene oxide (rGO) nanocomposite-based non-enzymatic electrochemical biosensors were prepared to investigate the detection performance of the glucose. The PAN-rGO nanocomposite-based biosensor detected glucose with a high sensitivity and stability due to enhanced redox mechanism arising from rGO additive. PAN-rGO nanocomposite-based biosensor detected glucose in (0.75–12) mM with a high sensitivity of 49 $\mu AmM^{-1}\ cm^{-2}$ (2.5 times higher than PAN-based sensor). Concentration–response graphs correlating the non-enzymatic electrochemical signal to glucose concentration revealed a low limit of detection (LOD) of 0.6 mM within 1-min voltammetric cycle. The selectivity results confirmed a significant preferential response of the proposed PAN-rGO nanocomposite-based biosensor for glucose against possible interfering compounds. The proposed PAN-rGO nanocomposite-based biosensor has a great potential to be used as a nanostructured platform for detection of glucose in phosphate-buffered saline (pH 7.4) solution with high sensitivity, selectivity, stability, reproducibility, and fast response properties.

Address correspondence to E-mail: selcan@iuc.edu.tr; nevintasaltin@maltepe.edu.tr

https://doi.org/10.1007/s10854-022-08694-9

1 Introduction

Glucose is one of the main clinical biomarkers that can lead to microvascular or macrovascular complications of diabetes. With the advantages of developed electronic devices, various biosensor applications have become attractive issues with excellent electrochemical performances against biomarkers and molecules in biomedical applications. The development of sensitive, stable, and rapid-operating electrochemical sensors is a critical issue as urgent medical attention is required when blood glucose concentration is higher than the (1–12) mM range. Up until now, many techniques such as colorimetric, chemiluminescence, optical, fluorescence, and non-enzymatic or enzymatic electrochemical methods have been developed to detect glucose levels in blood or urine samples. Among different advanced biomedical techniques, nanomaterial-based biosensors have attracted significant attention due to their excellent properties against target analytes [1–5]. The advantages of non-enzymatic electrochemical-based biosensors for rapid, portable, low-cost, sensitive, selective, short response time, and easy-to-use glucose detection have brought about the development of modern sensor technology [5–20].

Metals such as manganese (Mn), copper (Cu), zinc (Zn), and nickel (Ni) and polymers such as PANI are commonly used in enzymatic and non-enzymatic electrochemical biosensors for the direct electrooxidation of glucose. In enzymatic electrochemical glucose sensors, in general, glucose oxidase (GOx) specifically catalyzes the oxidation of glucose to gluconolactone [21–26]. Due to the PANI is directly involved in glucose oxidase, the sensitivity and selectivity of the PANI-based sensor are improved by adding carbon nanotubes (CNTs), graphene, GO, and Fe_2O_3 nanomaterials with controllable morphologies [27–33]. Based on the review of the available literature, Wu et al. [34] prepared a PANI/TiO_2/rGO-based glucose biosensor, the biosensor detected 0.047 ng mL^{-1} glucose. In another study, Feng et al. [35] developed a PANI-graphene-based glucose biosensor, the biosensor detected glucose in the range of 10 μM–1.48 mM with a sensitivity of 22 μA mM^{-1} cm^{-2}. The study conducted by Tang et al. [36] showed that a novel TiO_2/PANI-GO-based glucose biosensor detected glucose in the range of 0.02–6 mM with a sensitivity of 6.3 μA mM^{-1} cm^{-2}.

Zhai et al. [37] prepared a GO/Au/PANI Pt/graphene/P (1,5-DAN)-based glucose biosensor, the biosensor detected glucose in the 0–60 mg mL^{-1} range. In these studies, it has been reported that by adding the metal nanomaterials in PANI, high surface area, high surface reaction activity, and high sensitivity were obtained. The glucose detection performance of polyacrylonitrile (PAN) was also investigated. There are only three reports in the literature on PAN-based electrochemical glucose biosensors, and these biosensors are enzymatic electrochemical glucose biosensors [38–40]. In one of these studies, microporous PAN was synthesized using a single rare earth catalyst-Y$(OAr)_3$ and coated on a Pt electrode. It has been reported that upon the electrochemical adsorption of glucose oxidase in PAN, enzyme-catalyzed reaction occurred, and the biosensor detected glucose in the range of (1–10 mM) in 20 s with a sensitivity of 4.2 mA mM^{-1} cm^{-2}. In the other two studies, the PANI-PAN was used. In one of these studies, the biological film was coated on a PANI-PAN nanocomposite Pt electrode with the electropolymerization method. The sensing structure exhibited good selectivity, sensitivity, and stability with no loss of activity after 100 days of sequential measurement and intermittent use with storage in phosphate-buffered saline (PBS) at 4 °C. It has been reported that the biosensor detected glucose in the range of (2μM–12mM) in 30 s with a sensitivity of 67 mA mM^{-1} cm^{-2} via enzyme-catalyzed reaction [41]. However, the glucose sensing performance of the biosensor at room temperature has not been reported. In the other study, PAN was synthesized using the single rare earth catalyst-Y$(OAr)_3$, and then a biosensor was prepared by immobilizing glucose oxidase to PAN-PANI-graphene nanocomposite. Several layers of graphene were prepared by the electrochemical process of graphite in propylene carbonate electrolyte. It has been reported that the biosensor detected low concentration glucose in the range of (0.01–1.97 mM) in 30 s with a sensitivity of 29 mAmM^{-1} cm^{-2} [42], the glucose sensing performance of the biosensor in the critical (2–12mM) range has not been reported.

There is no report on the PAN-rGO-based non-enzymatic electrochemical glucose biosensor. The existence of fixed results that need to be focused on this issue, experimental steps, and the need to reduce their costs have been driving forces and associated assumptions for the production of the advanced

sensitive, selective, non-enzymatic, and disposable biosensors. The novelty of this study lies in the development of the PAN-rGO nanocomposite-based biosensor for the high-performance non-enzymatic electrochemical detection of glucose with high sensitivity, selectivity, stability, reproducibility, and fast response properties in the phosphate-buffered saline (PBS) (pH 7.4) solution.

2 Experimental

2.1 Materials

PAN (molecular weight: ~150.000 g mol^{-1}) was purchased from Sigma Aldrich Company (Germany). N-N-Dimetylformamide (DMF) (≥ 99.8%), NaOH, HCl, ethanol (≥ 99.9%), and potassium permanganate ($KMnO_4$) (molecular weight: 158.03 g/mol) were purchased from Merck Company (Germany). Electrochemical transducers were purchased from Ebtro Electronics. All chemicals and reagents were used without further purification.

2.2 Characterization

All samples were characterized using different techniques such as scanning electron microscopy (SEM) (FEI QUANTA 450 Model), Raman (Renishaw in via Raman microscope), and Fourier transform infrared spectroscopy (FTIR) (ATR-Perkin Elmer Spectrum Two Model) in the frequency range from 4000 to 400 cm^{-1} with a resolution of 4 cm^{-1}.

2.3 Preparation of PAN-rGO nanocomposite

50 g of graphite powder was sonicated in 500 mL of distilled water in a nitrogen-controlled environment at room temperature for 1 h. The solution was centrifuged at high speed (at 10,000 rpm) for 30 min. 50 mL of $KMnO_4$ was added to the solution and sonicated at 40 kHz for 1 h. 10 mL of 0.01 M HCl was added to the solution and then NaOH and ethanol were added until the pH reached 7. The solution obtained was filtered and dried in a microwave at 2450 MHz oven to obtain rGO powder.

2.4 Preparation of PAN and PAN-rGO nanocomposite-based non-enzymatic electrochemical biosensors

In this study, the PAN-rGO nanocomposite was obtained at the 1:1 mass ratio for PAN:rGO using a simple sonication method. 1 mg of rGO and 1 mg of PAN were first rapidly stirred in the solvent DMF for 15 min and then the solution was sonicated at 50 W for 15 min to obtain the PAN-rGO nanocomposite. The electrochemical measurements of the non-enzymatic glucose biosensor were implemented with a electrochemical a Ebtro voltammetric electrochemical workstation using the three-electrode cyclic voltammetry system. The PAN-rGO nanocomposite-based electrode was employed as the working electrode (WE). 25 µL of PAN and PAN-rGO nanocomposite was coated on gold electrochemical transducers using a simple drop-casting method and then the films were dried at 40 °C. The detection of the PAN-rGO nanocomposite-based non-enzymatic electrochemical biosensors was analyzed via cyclic voltammetry, which was carried out in (0.75–12) mM different analytes such as glucose, maltose, fructose, and urea solution with the potential range of − 1.0 to +1.0 V at 50 mV s^{-1} scan rate.

3 Results and discussion

3.1 Characterization of PAN-rGO nanocomposite

The surface morphology analysis of rGO and PAN-rGO nanocomposite was examined by SEM technique, as given in Fig. 1a and b. According to the surface characterization results of rGO, it was observed that the rGO had a uniform multi-layered nanosheet structure (Fig. 1a). From SEM micrograph (Fig. 1b) and 3D surface plot of SEM micrograph (Fig. 1c) of the prepared PAN-rGO nanocomposite, it was clear that the irregular morphology of the nanocomposite was observed having porous structure with its particle size ranging from 50 to 100 nm. Furthermore, it was seen that the rGO additive was clearly well dispersed in the PAN matrix and the prepared nanostructure was homogeneously decorated with rGO additives. Briefly, the granular morphology was revealed the successful formation of PAN particles on the surface of the rGO. The XRD

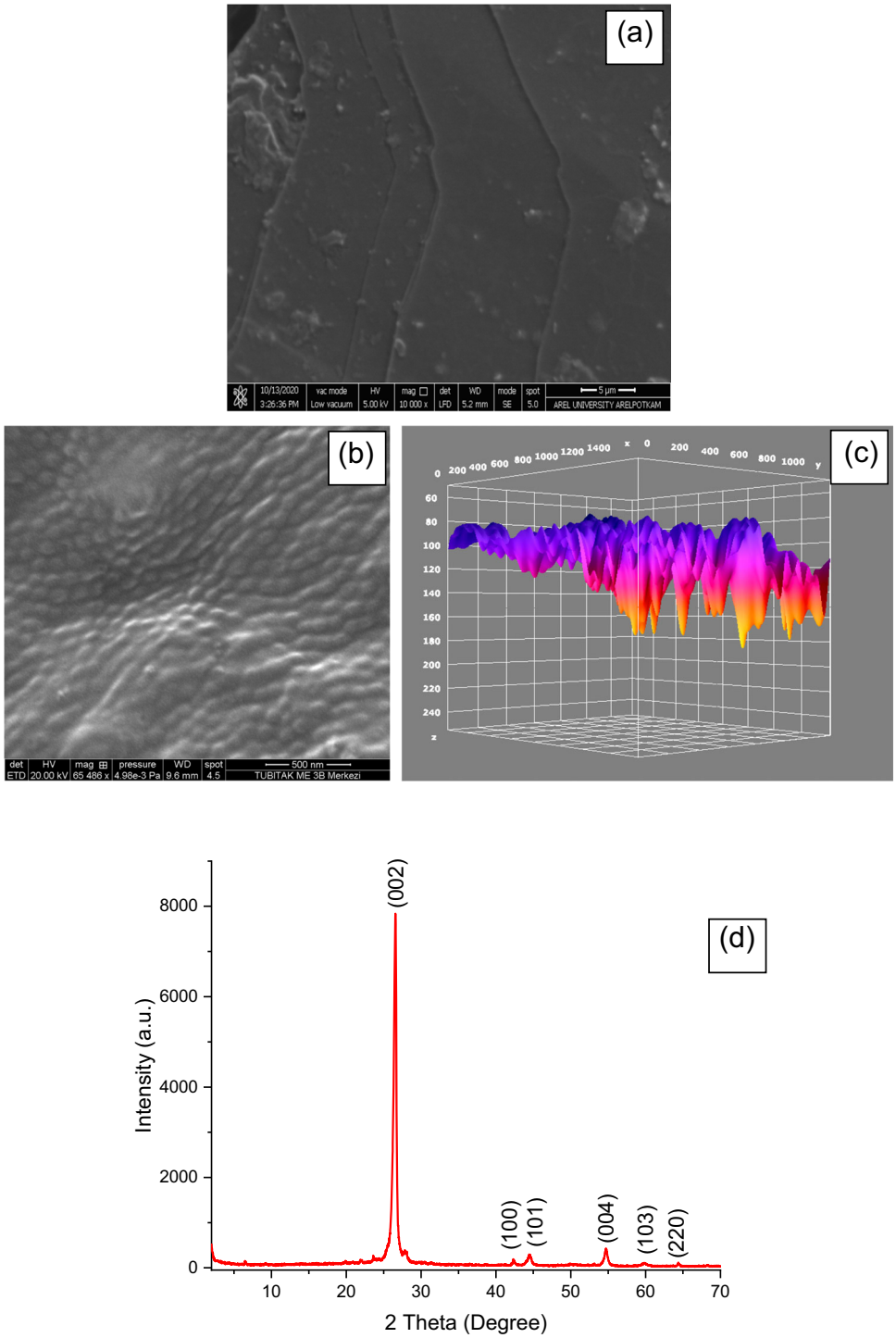

Fig. 1 **a** SEM images of **a** rGO and **b** SEM image, **c** 3D surface plot of SEM micrograph of PAN-rGO nanocomposite, and **d** XRD analysis of rGO

graph of rGO is given in Fig. 1d. The XRD patterns of the rGO can be indexed to (002), (100), (101), (004), (103), and (220) with JCPDS Card no. 19-0629.

Raman spectroscopy analysis results (ELaser = 532 nm) of rGO and PAN-rGO nanocomposite are given in Fig. 2. As shown in Fig. 2a, the G and D bands were located at 1589 cm^{-1} and 1345 cm^{-1} for rGO, respectively. In addition, The G band was clearly more intense than the D band. When PAN was added in the rGO, the Raman spectroscopy of the PAN-rGO nanocomposite bands shifted around ~8 cm^{-1}. These shifts indicated the existence of PAN in the PAN-rGO composite. Besides, as shown in Fig. 2b, the Raman band at 1345 cm^{-1} was observed a

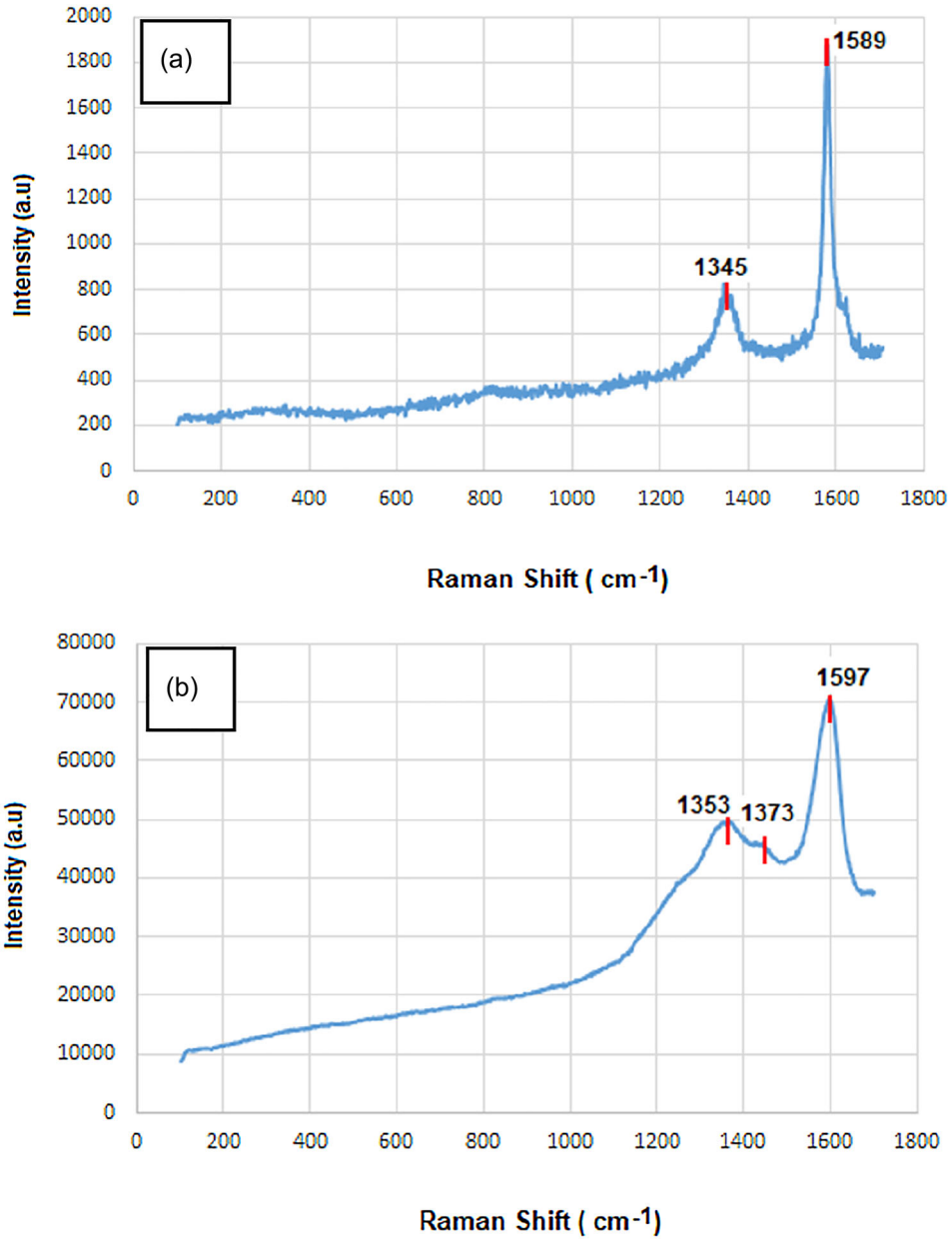

Fig. 2 Raman spectra of **a** rGO and **b** PAN-rGO nanocomposite

broader band than according to the Fig. 2a and it possessed a shoulder at 1373 cm^{-1} [43].

FT-IR results of the GO and PAN-rGO nanocomposite are presented in Fig. 3. The characteristic peaks of PAN at 2243.30 cm^{-1}, 1738.10 cm^{-1}, and 1233.50 cm^{-1} were assigned to C≡N, C–N stretching, and C–O), respectively. In our previous study, we reported the FTIR results of the rGO [44]. In Fig. 3b, the characteristic peaks of the rGO were observed at 1043.2 cm^{-1} (C–O–C), 1279.1 cm^{-1} (C–OH), 1635.3 cm^{-1} (C=C), and 3214.0 cm^{-1} (O–H group), respectively [45, 46]. In Fig. 3c, the characteristic peaks of the PAN-rGO nanocomposite were found at 1053.0 cm^{-1} (C–O–C), 1233.5 cm^{-1} (C–OH), and 3508.1 cm^{-1} (O–H group), respectively. Moreover, new peaks of the PAN-rGO nanocomposite were observed at 1452.7 cm^{-1} (C–H bending in CH_2), 1738.1 cm^{-1} (C=O stretching), 2243.3 cm^{-1} (–CN groups), and 2998.1 cm^{-1} (C–H stretching in CH_2) due to the interaction between PAN matrix and rGO [47, 48]. However, similar characteristic peaks of PAN and PAN-rGO nanocomposite were observed in FTIR results. We thought that it was related to the

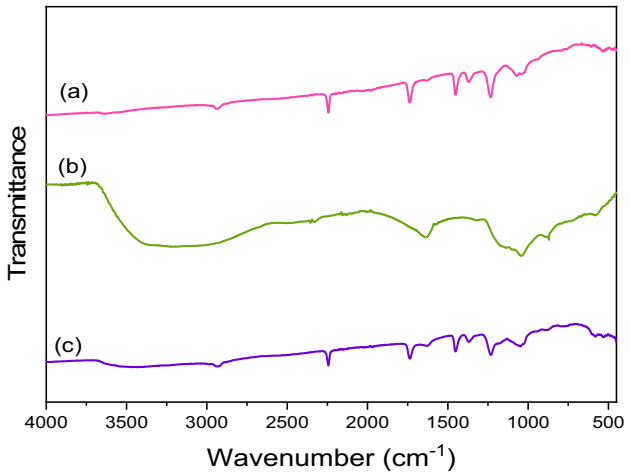

Fig. 3 **a** FTIR results of **a** PAN, **b** rGO, and **c** PAN-rGO nanocomposite

coating of rGO with PAN and the poor interaction between the polymer and rGO [49].

3.2 The electrochemical performance of PAN-rGO nanocomposite-based biosensor

This is the first report of preparation, structural characterization, and tests of a PAN-rGO nanocomposite-based non-enzymatic electrochemical glucose sensor. The tests were performed three times and all the results obtained the same. The sensor has a potential device for rapid, low-cost, sensitive, selective, stable diagnosis of diabetes. Non-enzymatic electrochemical measurements of PAN and PAN-rGO nanocomposite-based non-enzymatic electrochemical sensors against glucose were carried out in the potential from − 1.0 to 1.0 V in PBS at pH 7.4, at a scan rate of 50 mV s^{-1} (Fig. 4**)**. Based on the cyclic voltammograms measurements, the current density–voltage graphs of the prepared electrochemical sensors against glucose are given in Fig. 4a and b.

The peak current measured during voltammetry is reflected as a function of analyte concentration. The response of the sensors to the changes in the glucose concentrations represented by increase in the output current. Current peaks arose from redox reactions between the PAN-glucose and the nanocomposite-glucose. In this study, we prepared a series of glucose solutions with concentrations ranging between 0.75 mM and 12 mM to choose an optimal concentration of glucose for the sensitive non-enzymatic electrochemical detection using the PAN-rGO (1:1) nanocomposite-based biosensor. Current density–voltage curves of PAN-glucose nanocomposite-based sensor indicated a higher prominent redox peak for (0.75–12) mM glucose concentration range. Therefore, the results depict that PAN-rGO nanocomposite-based sensor detected glucose with higher sensitivity and stability due to enhanced redox mechanism arose from GO additive. PAN-rGO nanocomposite-based sensor detected glucose in (0.75–12) mM with a high sensitivity of 49 μAmM^{-1} cm^{-2} (2.5 times higher than PAN-based sensor) within 1-min voltammetric cycle (Fig. 4c). Limit of detection (LOD) of the sensor was calculated according to [50] and was found to be 0.6 mM. In Fig. 4c and d, the sensitivities of the sensors and selectivity of the prepared PAN-rGO nanocomposite-based sensor were presented. According to the experimental results, we found that the response reached a maximum at 12 mM. We also observed the current density–voltage graphs of the PAN-rGO nanocomposite-based sensor against glucose, maltose, fructose, and urea of 12 mM concentration. The *R*-squared (R^2) values, which are a measure of the linearity of the obtained data, are, respectively, as follows: 0.76 for PAN and 0.82 for PAN-rGO. The experimental results showed that the prepared PAN-rGO nanocomposite-based sensor is selective against glucose. We assumed that the possible non-enzymatic glucose sensing mechanism of the the prepared sensor was proposed to electrochemically oxidize from glucose to gluconolactone due to the electrode surface's chemical interaction between the glucose molecule and the PAN-rGO nanocomposite-coated electrode (Fig. 4e) [51–53]. Consequently, the PAN-rGO nanocomposite can be potentially promising smart candidates for the development of the non-enzymatic sensitive glucose biosensor and the glucose-level monitoring at the early stages of diabetes.

Obviously, it would be more accurate to evaluate the obtained LOD value as the effect of rGO on PAN and the increase in selectivity. On the other hand, the range in which glucose measurement is meaningful from a medical point of view is between 3.9 and 65.6mM [54]. Therefore, although very, very low LOD values seem like success, it is impossible to claim that this will help other parameters of the sensor.

The comparison of electrochemical sensing performance of the various electrodes for the glucose detection is given in Table 1. According to the obtained non-enzymatic electrochemical results, we

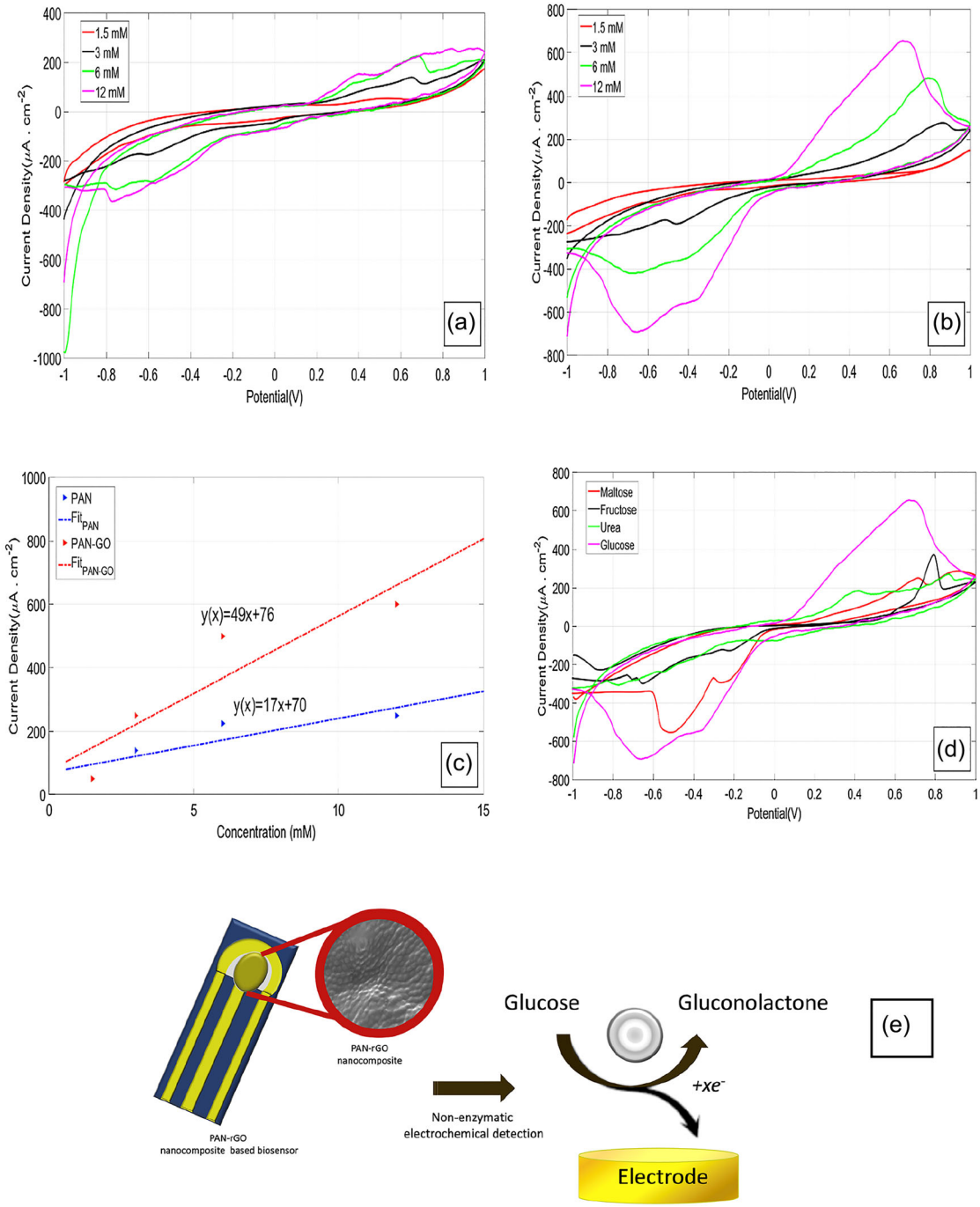

Fig. 4 Current density–voltage graph of the **a** prepared PAN-based sensor, **b** prepared PAN-rGO nanocomposite-based sensor, **c** the sensitivities of the sensors, **d** selectivity of the prepared PAN-rGO nanocomposite-based sensor, and **e** proposed sensing mechanism

can report the experimental study that the proposed PAN-rGO-based biosensor with excellent electrochemical results is an effective and selective glucose biosensor from a nanotechnological point of view. Future research will focus on the investigation of the design of novel multi-layered nanosheet-structured rGO-based biosensors for detection of drugs and biological molecules with their unique surface and chemical properties. In future study, we believe that conductive polymer multi-layered nanosheet-structured rGO composites-based biosensors require investigation to a greater extent with unique

Table 1 The comparison of electrochemical sensing performance of the various electrodes for the glucose detection

Sensors	LOD	Sensitivity	References
Graphene foam/hematite (GF/α-Fe2O3) nanowire arrays heterostructure nanocomposite (HNC)	71.6 μM	20.03 $\mu AmM^{-1}\ cm^{-2}$	[55]
Cyclodextrin modified carbon nanotubes	0.42 μM	32.28 $\mu AmM^{-1}\ cm^{-2}$	[56]
Modified pencil graphite electrodes	0.084 mM	8.08 $\mu W\ cm^{-2}\ mM^{-1}$	[57]
Single-walled carbon nanotubes-mesoporous silicon nanocomposite	9.6 μM	0.0614 $\mu AmM^{-1}\ cm^{-2}$	[58]
Composite montmorillonite/PAN nanofibers	4.2 and 2.4 μM	52 and 25 $mAmM^{-1}\ cm^{-2}$	[59]
Ag–Ni NPs loaded on MWCNTs	7.0 μM	1485 $\mu AmM^{-1}\ cm^{-2}$	[60]
PAN-rGO nanocomposite-based biosensor	0.6 mM	49 $\mu AmM^{-1}\ cm^{-2}$	This study

electrochemical properties such as low cost and flexibility in sensor and biomedical applications.

4 Conclusions

Multi-layered nanosheet-structured rGO and then PAN-rGO nanocomposite were prepared by ultrasonic method, respectively. After that, PAN and PAN-rGO nanocomposite-based non-enzymatic electrochemical sensors were prepared to investigate glucose detection performance. PAN-GO nanocomposite-based sensor detected glucose with higher sensitivity and stability due to enhanced redox mechanism arose from GO additive. PAN-rGO nanocomposite-based sensor detected glucose in (0.75–12) mM with a high sensitivity of 49 $\mu AmM^{-1}\ cm^{-2}$ (2.5 times higher than PAN-based sensor) within 1-min voltammetric cycle. Limit of detection (LOD) of the sensor is 0.6 mM. The results depict that PAN-rGO nanocomposite-based non-enzymatic electrochemical sensor is only glucose-selective. These electrochemical outputs may participate in the global marketplace and provide fruitful opportunities for future research in biomedical electronics.

Acknowledgements

This research was supported by TUBITAK Project 216M421.

Author contribution

SK contributed to conceptualization, methodology, and writing—original draft preparation. CT contributed to software and analysis. İG and GB contributed to analysis. NT contributed to conceptualization, methodology, writing—reviewing, and editing.

Data availability

The authors confirm that the data supporting the findings of this study are available within the article. Raw data that support the findings of this study are available from the corresponding author, upon reasonable request.

Declarations

Competing interest The authors declare that they have no conflict of interest.

References

1. X.F. Hoo, K. Abdul Razak, N.S. Ridhuan, N. Mohamad Nor, N.D. Zakaria, J. Mater. Sci. **30**, 8 (2019)
2. M.K. Anvarifard, Z. Ramezani, I.S. Amiri, K. Tamersit, A.M. Nejad, J. Mater. Sci. **31**, 24 (2020)
3. J. Liu, F. Yi, J. Mater. Sci. **30**(12), 11404 (2019)
4. A. Banerjee, S. Maity, C.H. Mastrangelo, Sensors **21**, 1253 (2021)
5. C. Dhand, M. Das, M. Datta, B.D. Malhotra, Biosens. Bioelectron. **26**, 2811 (2011)

6. M. Faruk Hossain, G. Slaughter, Bioelectrochemistry **141**, 107870 (2021)
7. J.R. Castle, W.K. Ward, J. Diabetes Sci. Technol. **4**, 221 (2010)
8. J.D. Newman, A.P.F. Turner, Biosens. Bioelectron. **20**, 2435 (2005)
9. Q. Dong, H. Ryu, Y. Lei, Electrochim. Acta **370**, 137744 (2021)
10. M. Gerard, A. Chaubey, B.D. Malhotra, Biosens. Bioelectron. **17**, 345 (2002)
11. A. Heller, B. Feldman, Acc. Chem. Res. **43**, 963 (2010)
12. A.I. Gopalan, K.P. Lee, D. Ragupathy, S.H. Lee, J.W. Lee, Biomaterials **30**, 5999 (2009)
13. S.M. Jebreiil Khadem, Y. Abdi, S. Darbari, F. Ostovari, Curr. Appl. Phys. **14**, 1498 (2014)
14. C.K. Zagal-Padilla, C. Diaz-Gómez, S.A. Gamboa, Mater. Sci. Semicond. Process. **137**, 106240 (2022)
15. W. Li, C. Sun, S. Yu, Z. Pu, P. Zhang, K. Xu, Z. Song, D. Li, Biomed. Microdevices **20**(4), 1 (2018)
16. N.H. Khand, I.M. Palabiyik, J.A. Buledi, S. Ameen, A.F. Memon, T. Ghumro, A.R. Solangi, J. Nanostruct. Chem. **11**(3), 455 (2021)
17. M. Dinesh, C. Revathi, Y. Haldorai, R.T. Rajendra Kumar, Chem. Phys. Lett. **731**, 136612 (2019)
18. Z.H. Li, X.L. Zhao, R.M. Song, C. Chen, P.J. Wei, Z.G. Zhu, Chem. Phys. Lett. **712**, 71 (2018)
19. M. Wang, F. Liu, D. Chen, J. Mater. Sci. **32**, 23445 (2021)
20. O.C. Pore, Av. Fulari, R.K. Kamble, A.S. Shelake, N.B. Velhal, V.J. Fulari, G.M. Lohar, J. Mater. Sci. **32**, 15 (2021)
21. H. Zheng, H. Xue, Y. Zhang, Z. Shen, Biosens. Bioelectron. **17**, 541 (2002)
22. E. Turkmen, S.Z. Bas, H. Gulce, S. Yildiz, Electrochim. Acta **123**, 93 (2014)
23. R. Sedghi, Z. Pezeshkian, Sens. Actuators B **219**, 119 (2015)
24. B. Zhang, Y. He, B. Liu, D. Tang, Microchim. Acta **182**(3), 625 (2014)
25. F.Y. Kong, S.X. Gu, W.W. Li, T.T. Chen, Q. Xu, W. Wang, Biosens. Bioelectron. **56**, 77 (2014)
26. Y. Xian, Y. Hu, F. Liu, Y. Xian, H. Wang, L. Jin, Biosens. Bioelectron. **21**, 1996 (2006)
27. X. Chen, J. Zhu, Z. Chen, C. Xu, Y. Wang, C. Yao, Sens. Actuators B **159**, 220 (2011)
28. C. Wang, L. Yin, L. Zhang, R. Gao, J. Phys. Chem. C **114**, 4408 (2010)
29. Y. Ding, Y. Wang, L. Su, M. Bellagamba, H. Zhang, Y. Lei, Biosens. Bioelectron. **26**, 542 (2010)
30. P. Najmi, N. Keshmiri, M. Ramezanzadeh, B. Ramezanzadeh, J. Taiwan Inst. Chem. Eng. **119**, 245 (2021)
31. P. Haldar, Electrochim. Acta **381**, 138221 (2021)
32. S. Saha, M. Mitra, A. Sarkar, D. Banerjee, S. Ganguly, K. Kargupta, Diam. Relat. Mater. **84**, 103 (2018)
33. V. Gupta, N. Miura, Electrochim. Acta **52**, 1721 (2006)
34. S. Wu, F. Su, X. Dong, C. Ma, L. Pang, D. Peng, M. Wang, L. He, Z. Zhang, ApSS **401**, 262 (2017)
35. X. Feng, H. Cheng, Y. Pan, H. Zheng, Biosens. Bioelectron. **70**, 411 (2015)
36. W. Tang, L. Li, X. Zeng, Talanta **131**, 417 (2015)
37. D. Zhai, B. Liu, Y. Shi, L. Pan, Y. Wang, W. Li, R. Zhang, G. Yu, ACS Nano **7**, 3540 (2013)
38. Y. Xie, T. Liu, Z. Chu, W. Jin, J. Electroanal. Chem. **893**, 115328 (2021)
39. J.H. Kim, D. Lee, T.S. Bae, Y.S. Lee, J. Ind. Eng. Chem. **25**, 192 (2015)
40. S.A. Hashemi, S.M. Mousavi, S. Bahrani, S. Ramakrishna, Eur. Polym. J. **138**, 109959 (2020)
41. H. Xue, Z. Shen, C. Li, Biosens. Bioelectron. **20**, 2330 (2005)
42. Z. Yan, H. Zheng, J. Chen, Y. Ye, Int. J. Electrochem. Sci. **14**, 3011 (2019)
43. A. Gao, D. Xu, C. Li, Y. Wang, L. Xu, Compos. Interface **28**, 159 (2020). https://doi.org/10.1080/09276440.2020.1732118
44. W.U. Arifeen, J. Choi, K. Yoo, J. Shim, T.J. Ko, Chem. Eng. J. **417**, 128075 (2021)
45. J. Lu, Y. Li, S. Li, S.P. Jiang, Sci. Rep. **6**, 1 (2016)
46. N. Taşaltın, S. Karakuş, C. Taşaltın, G. Baytemir, Food Chem. **372**, 131267 (2022)
47. B. Liu, H. Sun, T. Peng, X. Zhi, Diam. Relat. Mater. **118**, 108498 (2021)
48. K. Sudhakar, M. Suneetha, K.M. Rao, S.S. Han, Colloids Surf. A **628**, 127340 (2021)
49. M.E. Uddin, R.K. Layek, N.H. Kim, D. Hui, J.H. Lee, Compos. Part B **80**, 238 (2015)
50. A.G. Ayankojo, J. Reut, V. Ciocan, A. Öpik, V. Syritski, Talanta **209**, 120502 (2020)
51. G.A. Naikoo, H. Salim, I.U. Hassan, T. Awan, F. Arshad, M.Z. Pedram, W. Ahmed, A. Qurashi, Front. Chem. **9**, 786 (2021)
52. S. Guo, C. Zhang, M. Yang, L. Wang, R. Li, N. Ma, Mater. Chem. Phys. **278**, 125679 (2022)
53. D. Maity, C.R. Minitha, R.K. Rajendra, Mater. Sci. Eng. **105**, 110075 (2019)
54. K. Ueno, D. Chujo, N. Takahashi, M. Ohsugi, K. Ueki, H. Kajio, Diabetes Ther. **11**, 1883 (2020)
55. F. Güneş, A. Aykaç, M. Erol, Ç Erdem, H. Hano, B. Uzunbayir, M. Şen, A. Erdem, J. Alloys Compd. **895**, 162688 (2022)
56. J. Xia, B. Zou, F. Liu, P. Wang, Y. Yan, J. Food Compos. Anal. **105**, 104221 (2022)
57. Á Torrinha, M. Tavares, C. Delerue-Matos, S. Morais, Chem. Eng. J. **426**, 131835 (2021)

58. J. Ahmed, M.A. Rashed, M. Faisal, F.A. Harraz, M. Jalalah, S.A. Alsareii, Appl. Surf. Sci. **552**, 149477 (2021)
59. R.M. Apetrei, P. Camurlu, Electrochim. Acta **353**, 136484 (2020)
60. F. Akbar, M. Tariq, H.U. khan, J. Khan, M.K. Uddin, S.S. Ahmed, A. Rahim, J. Mater. Sci. **32**, 12 (2021)